Draft version June 25, 2020
Typeset using LaTeX **preprint2** style in AASTeX62

Discovery of a Sample of Helium-rich Superluminous Supernovae by Zwicky Transient Facility

Lin Yan,[1] D. A. Perley,[2] S. Schulze,[3] R. Lunnan,[4] J. Sollerman,[4] K. De,[5] Z. H. Chen,[6] C. Fremling,[5] A. Gal-Yam,[3] K. Taggart,[2] T. W. Chen,[4] I. Andreoni,[5] E. C. Bellm,[7] V. Cunningham,[8] R. Dekany,[1] D. A. Duev,[9] C. Fransson,[4] R. R. Laher,[10] M. Hankins,[5] A. Y. Q. Ho,[5] J. E. Jencson,[11] S. Kaye,[1] S. R. Kulkarni,[5] M. M. Kasliwal,[5] V. Z. Golkhou,[12,13] M. Graham,[5] F. J. Masci,[10] A. A. Miller,[14,15] J. D. Neill,[5] E. Ofek,[3] M. Porter,[1] P. Mróz,[9] D. Reiley,[1] R. Riddle,[1] M. Rigault,[16] B. Rusholme,[10] D. L. Shupe,[10] M. T. Soumagnac,[17,3] R. Smith,[1] L. Tartaglia,[4] Y. Yao,[5] and O. Yaron[3]

[1] *The Caltech Optical Observatories, California Institute of Technology, Pasadena, CA 91125, USA*
[2] *Astrophysics Research Institute, Liverpool John Moores University, 146 Brownlow Hill, Liverpool L3 5RF, UK*
[3] *Department of Particle Physics and Astrophysics, Weizmann Institute of Science, Rehovot 76100, Israel*
[4] *The Oskar Klein Centre, Department of Astronomy, Stockholm University, AlbaNova, SE-106 91 Stockholm, Sweden*
[5] *Division of Physics, Mathematics and Astronomy, California Institute of Technology, Pasadena, CA 91125, USA*
[6] *Physics Department and Tsinghua Center for Astrophysics (THCA), Tsinghua University, Beijing, 100084, China*
[7] *DIRAC Institute, Department of Astronomy, University of Washington, 3910 15th Avenue. NE, Seattle, WA 98195*
[8] *Department of Astronomy, University of Maryland, College Park, MD 20742, USA*
[9] *Division of Physics, Mathematics, and Astronomy, California Institute of Technology, Pasadena, CA 91125, USA*
[10] *IPAC, California Institute of Technology, 1200 E. California Blvd, Pasadena, CA 91125, USA*
[11] *Steward Observatory, University of Arizona, 933 North Cherry Avenue, Tucson, AZ 85721-0065, USA*
[12] *DIRAC Institute, Department of Astronomy, University of Washington, 3910 15th Avenue NE, Seattle, WA 98195*
[13] *The eScience Institute, University of Washington, Seattle, WA 98195, USA*
[14] *Center for Interdisciplinary Exploration and Research in Astrophysics and Department of Physics and Astronomy, Northwestern University, 1800 Sherman Ave, Evanston, IL 60201, USA*
[15] *The Adler Planetarium, Chicago, IL 60605, USA*
[16] *Université Clermont Auvergne, CNRS/IN2P3, Laboratoire de Physique de Clermont, F-63000 Clermont-Ferrand, France*
[17] *Lawrence Berkeley National Laboratory, 1 Cyclotron Road, Berkeley, CA 94720, USA*

Submitted to ApJL

Abstract

Helium is expected to be present in the ejecta of some hydrogen-poor superluminous supernovae (SLSN-I). However, so far only one event, PTF10hgi has been identified with He features in its photospheric spectra (Quimby et al. 2018). At $z = 0.0866$, ZTF19aawfbtg (SN2019hge) has more than 10 optical spectra at phases from -41 to $+103$ days. Most of these spectra match well with that of PTF10hgi, suggesting SN2019hge as the second case of a He-rich SLSN-I. Confirmation comes from its near-IR spectrum taken at $+34$ days, revealing He I features with P-Cygni profiles at 1.083

Corresponding author: Lin Yan
lyan@caltech.edu

and 2.058 μm. Using the optical spectra of PTF10hgi and SN2019hge as templates, we examine 70 SLSN-I discovered by ZTF in the first two years of operation and found additional five SLSN-I with distinct He-features, yielding a lower limit to the He-rich fraction of $\sim 9\%$. It is suggested that the excitation of He I atoms requires non-thermal radiation. These He-rich events can not be explained by traditional ^{56}Ni mixing model because of their blue spectra, high peak luminosity and slow rising time scales. Magnetar models offer a possible solution since pulsar winds naturally generate high energy particles as sources of non-thermal excitation. However, how the magnetar energy is transported to the outer layers is unclear. An alternative model is ejecta interaction with H-poor CSM which may be supported by the observed light curve undulations.

Keywords: supernovae: individual PTF10hgi, SN2019hge (ZTF19aawfbtg), SN2018kyt (ZTF18acyxnyw), SN2019gam (ZTF19aauvzyh), SN2019kws (ZTF19aamhhiz), SN2019unb (ZTF19acgjpgh), SN2019obk (ZTF19abrbsvm)

1. Introduction

Massive stars with $M \geq 8\,M_{\odot}$ end their lives as explosions of core-collapse supernovae (CC SNe). The variety of CC SNe is largely determined by the mass loss history of the progenitor star. If hydrogen layers are still present when the stars explode, the resulting supernovae will have hydrogen features in their spectra, thus being classified as Type II CC SNe. Hydrogen-poor CC SNe (Type I) originate from massive stars that have lost most or all of their H envelopes prior to explosion. These include SNe IIb (some H & He), SNe Ib (no H, some He), and SNe Ic (no H, no He) (Filippenko 1997).

The initial detection of helium features in SNe Ib/IIb has instigated various modelings including radiative transfer calculations. For example, the He I λ5876 transition is between energy levels of $1s2p\ ^3p^0$ and $1s3d\ ^3D$. To reach these excited states from the ground state ($1s^2$) requires at least 20.9 eV, corresponding to $\sim 2.4 \times 10^5$ K. As noted by, *e.g.* Dessart et al. (2012) and Lucy (1991), γ-ray photons from ^{56}Ni decay can produce high-energy electrons via Compton scattering. These non-thermal electrons are a source of heat, critical for powering the light curve, as well as a source of non-thermal excitation and ionization for the production of optical He I lines observed in SNe Ib/IIb. The key here is to transport ^{56}Ni from the inner ejecta to the outer layer where helium material is located. Thus the concept of the ^{56}Ni "mixing" is important for SNe Ib/IIb (Dessart et al. 2012).

Since its first discovery more than fifteen years ago (Quimby et al. 2007), the number of superluminous supernovae (SLSNe) has accumulated to more than 200. A large fraction of low-z events are from two all sky transient surveys, Palomar Transient Factory (PTF; Law et al. 2009) and Zwicky Transient Facility (ZTF; Graham et al. 2019; Bellm et al. 2019). Over $10-100$ times more luminous than normal CC SNe, superluminous supernovae are recognized as explosions of massive stars where sustaining of the optical emission requires additional power besides radioactive material (Quimby et al. 2011; Kasen & Bildsten 2010; Yan et al. 2015; Woosley 2017). Similar to normal CC SNe, SLSNe are also broadly classified into two classes – hydrogen poor, SLSN-I and hydrogen rich, SLSN-II (Gal-Yam 2012).

Although hydrogen-poor SLSN-I normally do not show H-features in their spectra, a small fraction, $\sim 10-30\,\%$ have broad Hα emission (several 1000 km s^{-1}) at $> +100$ days post-peak, presumably produced by ejecta interaction with H-rich circumstellar material (CSM) (Yan et al.

2015, 2017a). Such cases suggest that their progenitor stars must have lost their H-envelope shortly before the explosions. The implication is that some helium is likely in the ejecta because there is not enough time to completely strip-off the helium layer. However, SLSN-I spectral observations have not revealed the presence of helium, except for PTF10hgi. Quimby et al. (2018) carried out a comprehensive spectral analysis of the entire PTF SLSN-I sample, and identified one event, PTF10hgi, as a SLSN-IIb, with clear He I λ5876, 6678, 7065, 7281 at $\sim$ 7000 km s^{-1}, and Hα with P-Cygni profile with a velocity of 10000 km s^{-1} at +47 days. The presence of Hα got a further support from a possible Hα emission among a complex emission structure around [O I] λ6300 and Hα in the spectrum at +314 days. We note here that initially SN2012il was thought to have He I 1.08μm feature (Inserra et al. 2013), however Quimby et al. (2018) pointed out that the feature is unlikely He I, but may be broad nebular H emission.

With the large sample of SLSN-I discovered and spectroscopically confirmed by ZTF (Lunnan et al. 2019; Perley et al. in prep; Chen et al. in prep), we examine our large spectral dataset, and aim to address if there are other He-rich SLSN-I similar to PTF10hgi. If such a subclass of events exists, it highlights the question of how helium atoms are excited and ionized. This will have important implications for the physical nature of SLSN-I.

This paper is organized as following. §2.1 and §2.2 present the optical and near-IR data for SN2019hge (ZTF19aawfbtg). §3 discusses the sample of SLSN-Ib/IIb events. The paper ends with §4 on the discussion of the key results and their implications. Throughout the paper, all magnitudes are in the AB system unless explicitly noted otherwise. We adopt the ΛCDM cosmology with $H_0 = 67.4\,\mathrm{km\,s^{-1}\,Mpc^{-1}}$, $\Omega_M = 0.315$ and $\Omega_\Lambda = 0.685$ (Planck Collaboration et al. 2018).

2. Spectral Classification of SN2019hge (ZTF19aawfbgt) as a SLSN-Ib

2.1. Optical Spectra

Optical spectra of SN2019hge were obtained at −41 to +103 days from the g-band peak using the low resolution ($R \sim 100$) Spectral Energy Distribution Machine (SEDM; Blagorodnova et al. 2018) and the Double Beam Spectrograph (DBSP; Oke & Gunn 1983) on the Palomar 60 inch and 200 inch telescope respectively, as well as the Low Resolution Imaging Spectrometer (LRIS; Oke et al. 1995) on the Keck telescope. The spectral reductions use the SEDM pipeline, *pyraf-dbsp* and *lpipe* packages provided by Rigault et al. (2019); Bellm & Sesar (2016); Perley (2019). Applying *Superfit* (Howell et al. 2013) with the enhanced SLSN spectral templates from Quimby et al. (2018), we find that the SN2019hge spectra at $\geq$ −26 days have the top 5 matches with PTF10hgi. Figure 1 compares the spectra of SN2019hge with that of PTF10hgi and a low luminosity Type Ib SN 2005bf (Folatelli et al. 2006), revealing many similarities between these three events, specifically the four He I features at 5876, 6678, 7065 and 7281 Å blue-shifted with a velocity of $\sim$ 7000 km s^{-1}. We do not consider He I λ3886, 4472 as the primary classification lines because of strong contamination from Ca II λ3934, 3969 (H+K lines) and Mg II λ4481. Of the four He features in Figure 1, He I λ5876 is strong with a well defined absorption profile, however, it could have some contamination from Na I λ5890. The other three features are weak, but He I λ7065 is well isolated. Therefore, the key to identify He-rich events relies on the presence of multiple He features, as demonstrated in the classification of normal SNe Ib/IIb (Modjaz et al. 2014).

PTF10hgi has He I and Hα velocities of 7000, and 10,000 km s^{-1} respectively, making it a SLSN-IIb (Quimby et al. 2018). In SN2019hge, hydrogen features are not as clear. In Fig-

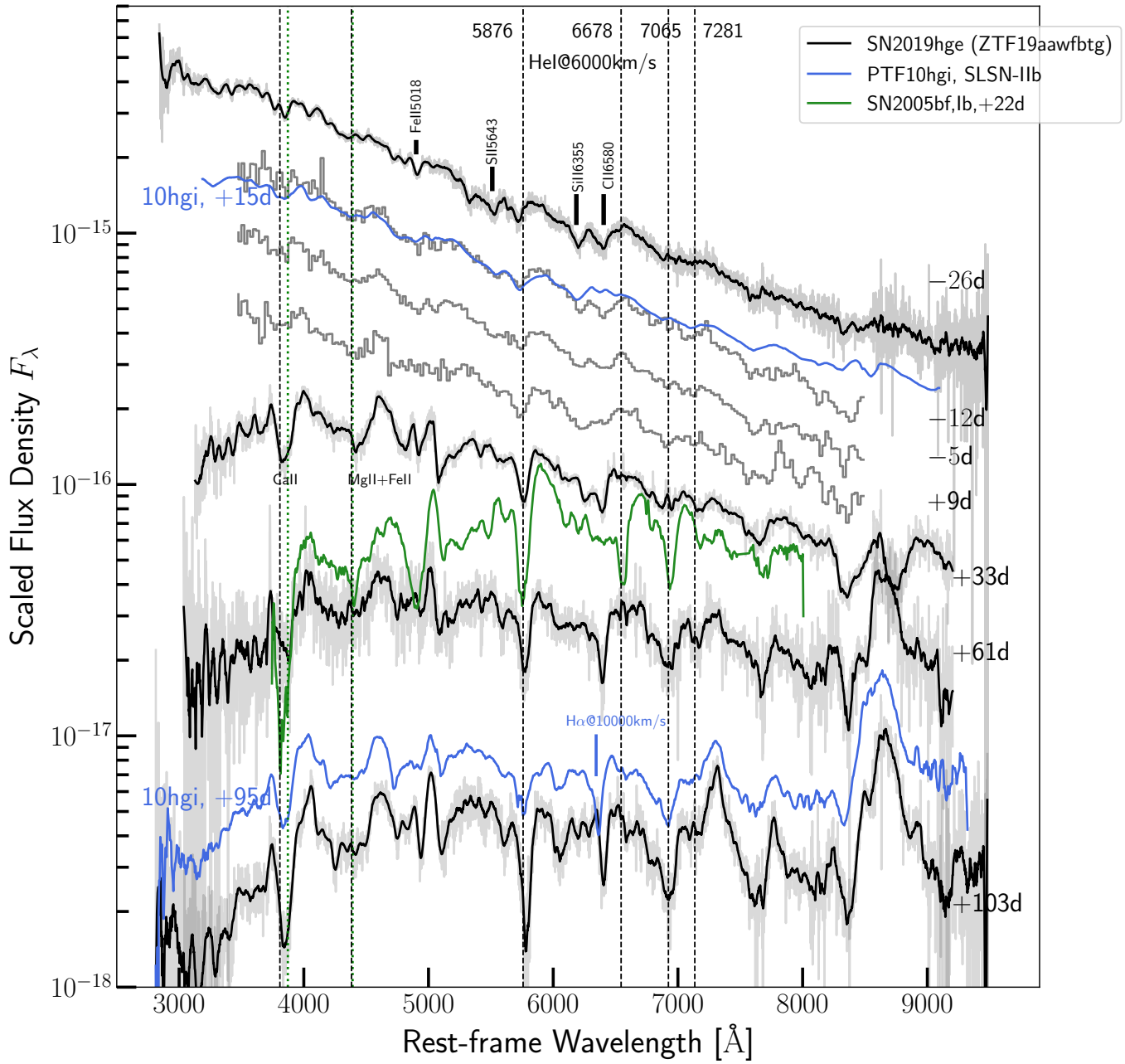

Figure 1. The SN2019hge (ZTF19aawfbtg) spectra around peak and late phases. The comparison is made to that of PTF10hgi (blue) and SN 2005bf (green). The vertical dashed lines mark the locations of He I λ5876, 6678, 7065, 7281 at a velocity of 7000 km s^{-1}.

ure 1, we marked the two features blue-ward of He I λ6678 as C II λ6580 and Si II λ6355. If these were Hα, the velocity would be either too low ($\sim$ 7800 km s^{-1}) or too high ($\sim$ 17,000 km s^{-1}). We conclude that SN2019hge is a H-poor and He-rich event.

2.2. *Near-IR spectral confirmation of helium in SN2019hge*

Because of the high expansion velocity of the ejecta, absorption features in optical supernova spectra are broad and tend to be blended, making secure line identifications tricky. One way to confirm our classification is to use near-IR spectra.

SN2019hge was observed at +34 days with the Near-Infrared Echellette Spectrometer (NIRES; Wilson et al. 2004), a prism cross-dispersed near-infrared spectrograph mounted on the Keck 2 telescope. This spectrograph has a resolution of $\sim$ 2700, simultaneously covers the YJHK bands with a wavelength range of $0.8 - 2.4\,\mu$m. The spectral reduction uses *Spextool* and *Xtellcor* by Cushing et al. (2004); Vacca et al. (2003). The data is shown in Figure 2, where the prominent feature at 1.08 μm is likely He I 1.08303 μm with P-Cygni profile. This is confirmed by the presence of He I 2.05813 μm, a relatively isolated line. For comparison, we also plot the near-IR spectrum of SN 2008ax, a SN IIb at -8 days from the B-band peak (Taubenberger et al. 2011). In Figure 2, we shift the spectrum of SN 2008ax to a velocity of 6000 km s^{-1}. The match between SN2019hge and SN2008ax is very clear, including weak Mg I 1.1828,1.2083 μm doublet.

Assuming the minimum near 1.08μm is due to the P-Cygni profile of He I 1.08303 μm, the implied velocity is 8000 km s^{-1}, as marked in green dashed vertical lines in the two panels in Figrue 2. Similarly, the He I 2.05813 μm P-Cygni profile gives a velocity of 6000 km s^{-1}, consistent with that derived from He I λ5876 at the similar phase of +33 day. It is possible that near-IR He I could have higher velocities than that of optical He I lines because of their lower excitation. The lower velocity of He I λ2.058 μm could be due to its weaker and noisier feature. An alternative explanation is that He I 1.083 μm could be blended with C I 1.0691 μm at 6000 km s^{-1}, which would broaden and shift the minimum to shorter wavelengths. C I features are also present in the optical spectra at similar phases. The strong 1.08 μm features in normal SNe Ib/Ic could have contributions from He I, C I, Mg II and Si I (Hunter et al. 2009; Taubenberger et al. 2011). However, unlike SNe Ib, normal SNe Ic do not have He I 2.058 μm (Taubenberger et al. 2011).

If hydrogen is present in the ejecta, Paγ at 1.0941 μm would imply a velocity of 11,000 km s^{-1}. Although this velocity is higher as expected, the presence of Paγ is not corroborated by Hα and Hβ in the optical spectra. In summary, the optical and near-IR spectra suggest that SN2019hge is a He-rich event.

3. A sample of He-rich SLSN-I from ZTF

Assuming that optical spectra of PTF10hgi and SN2019hge can be used as templates to classify SLSN-Ib/IIb, we search for additional sources among the ZTF SLSN-I discovered during the first two years of the survey. Figure 3 displays the spectra of six SLSN-I which are matched well with that of PTF10hgi, including SN2019hge. For these six ZTF events, their post-peak spectra are all matched with that of PTF10hgi among the top 5 ranks when we run *Superfit*. Figure 3 compares these six events with PTF12dam (Quimby et al. 2018), an archetypal SLSN-I. Near $\lambda \sim 5876$ Å (He I), PTF12dam does not show a distinctive absorption feature, but a smooth and wide trough suggesting a blend of many lines. This is in contrast with the strong, narrow, and well defined absorption features at 5876 Å detected in other six ZTF events. More importantly, three

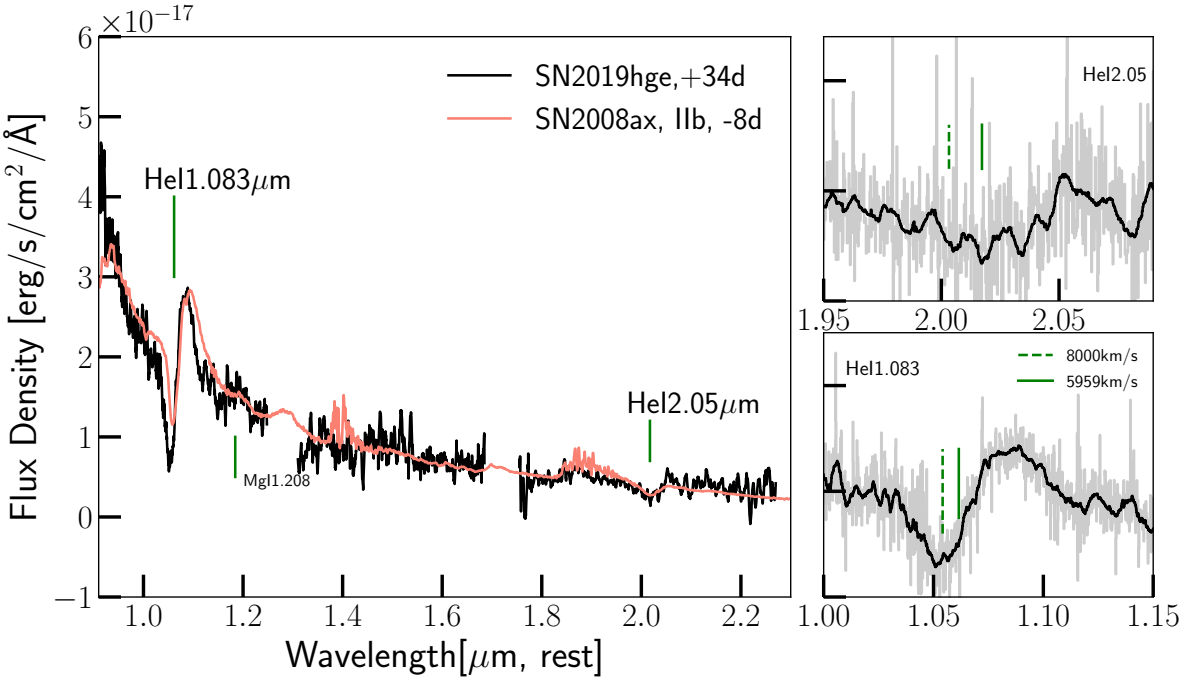

Figure 2. The Near-IR spectrum of SN2019hge taken at +34 rest-frame days after the g-band peak date. The two panels on the right show the zoomed-in view of the two He I features. The vertical dashed and solid green lines mark two different blue-shift velocities, 5960 km s^{-1} measured from the optical spectrum at +33 days, and 8000 km s^{-1} which matches the minimum of the He I λ1.083μm. The pink line is the spectrum of SN 2008ax, a SN IIb at −8 days from the B-band maximum light (Taubenberger et al. 2011). The SN 2008ax spectrum is shifted to match the velocity of 6000 km s^{-1}.

other He I lines at 6678, 7065 and 7281 Å are also present, albeit with various strength. Considering that He-rich material in SN2019hge is confirmed by its near-IR spectrum, we conclude that the other five events are good SLSN-Ib/IIb candidates. In Figure 3, we note that SN2018kyt (ZTF18acyxnyw) may have Hα at $\sim +10,000$ km s^{-1}, a He-rich event with a potentially small amount of H, similar to PTF10hgi.

If the feature at 5876 Å is indeed blue-shifted He I, we can measure the out-flowing velocity V as well as the velocity dispersion by fitting a Gaussian profile to each feature. Figure 4, top panel, shows the He I velocities as a function of time, slowing down roughly linearly with time. The velocity decreased by 3000 km s^{-1} over 125 days. For comparison, the He I velocities in normal SNe Ib and IIb evolve much faster, as expected. Finally, the He I line velocity dispersion, *i.e.* the line width, are $\sim$ 2000 km s^{-1}, remaining roughly constant over the same period of time. This is much less than that of bulk velocity, explaining the narrow appearance of He I λ5876 line.

In addition, four of these six He-rich events have *Swift* UV photometry, and the blackbody temperatures are measured from fitting the broad band UV + optical spectral energy distributions with a modified blackbody function of $B'_\lambda = (\frac{\lambda}{\lambda_0})^\beta \times B_\lambda(T_{BB})$, where $\lambda_0 = 3000$ Å, and β and T_{BB} are derived from the fit (details in Chen et al. in prep). The rationale for this function is to take into account of various degrees of SED suppression at far to near-UV due to metal line blanketing, as shown by the *HST* far-UV spectra of SLSN-I (Yan et al. 2017b, 2018). Figure 4, bottom panel, shows T_{BB} vs. phases, illustrating that at pre-peak early phases, T_{BB}

can reach as high as 12,000 K, commonly seen among SLSN-I (Quimby et al. 2011; Inserra et al. 2013; Nicholl et al. 2017; Chen et al. 2017).

Two outstanding features of this sample are shown by the light curves (LC) of the five events with good phae coverage from this sample, as in Figure 5. Here the LCs were constructed using the ZTF forced photometry utility [1] and additional code from Yao et al. (2019) based on the reference subtracted images from the ZTF image reduction pipeline (Masci et al. 2019). The first worth-noting feature is the prominent LC undulations in four of the six ZTF events (other two have poor LC coverage). The physical interpretation is not clear, and could have multiple explanations, such as interaction or change in opacity. The second is the relatively low peak luminosity, all in the range of -19.8 and -20.2 mag, for a sample of slow evolving SLSNe-I with rising time scales of $35-68$ days. Table 1 lists the name, coordinate, redshift (z) and g-band absolute peak magnitude (M_g). Here the extinction and K-corrections are included. This is in contrast to a much wider range of luminosity, -20 to -23 mag, normally occupied by SLSN-I.

4. Discussion and conclusions

The main result of this paper is the discovery of a sample of He-rich SLSN-Ib/IIb. Based on these six ZTF events, the percentage of He-rich SLSN-I is $\sim 9\%$. This is just an observed fraction of SLSN-I. Detailed calculations of the volumetric rates including incompleteness are outside the scope of this paper and will be discussed in a separate publication.

Helium is expected to be present in the ejecta of some massive stars if the stripping of the outer envelopes is incomplete. The detection of late-time, broad Hα emission in several PTF SLSN-I (Yan et al. 2015, 2017a) has provided the first evidence that some massive stars have lost their H-envelope shortly (< a few decades) before the supernova explosion, and never had enough time to also lose their helium layers. The fraction of SLSN-I with late-time Hα emission is roughly 10-30% (Yan et al. 2017a).

Our result has important implications to both the mass loss history of progenitor stars as well as the power mechanism of SLSN-I. First, He I excitation energy is high. For normal SNe Ib/IIb, the non-thermal excitation is achieved by "mixing" which transports ^{56}Ni from the interior to the outer parts of ejecta (Lucy 1991; Dessart et al. 2012). This solution is unlikely to work for these SLSN-Ib because having ^{56}Ni as the sole power source would require extremely large ^{56}Ni masses in order to also explain the observed LCs with high peak luminosity and long rise time scales. Furthermore, Fe-group elements from ^{56}Ni decay will produce significant line blanketing in the UV/optical wavelength, leading to red spectra, in contrary to our observations (Figure 1). This argument also rules out instability supernova (PISN; Woosley et al. 2007). For SLSN-I, central engine models such as magnetar or blackhole fall-back offer a natural source of high energy particles from either pulsar wind or outflow from accretion disk. These outflow winds will interact with the inner regions of ejecta, producing shocks and X-rays. There are two spectral formation models for SLSN-I. One by Mazzali et al. (2016) assumes X-rays from shocks driven by magnetar wind as a source of non-thermal excitation. The other by Dessart (2019) adopts a sustained magnetar energy injection profile (spatial). Both models are able to explain the hall-mark O II absorption features at 3500 - 4500Åand even produce He I λ5876 Å. However, both models do not deal with the dynamic processes of magnetar wind propagating through the ejecta. So the details of how mag-

[1] http://web.ipac.caltech.edu/staff/fmasci/ztf/forcedphot.pdf

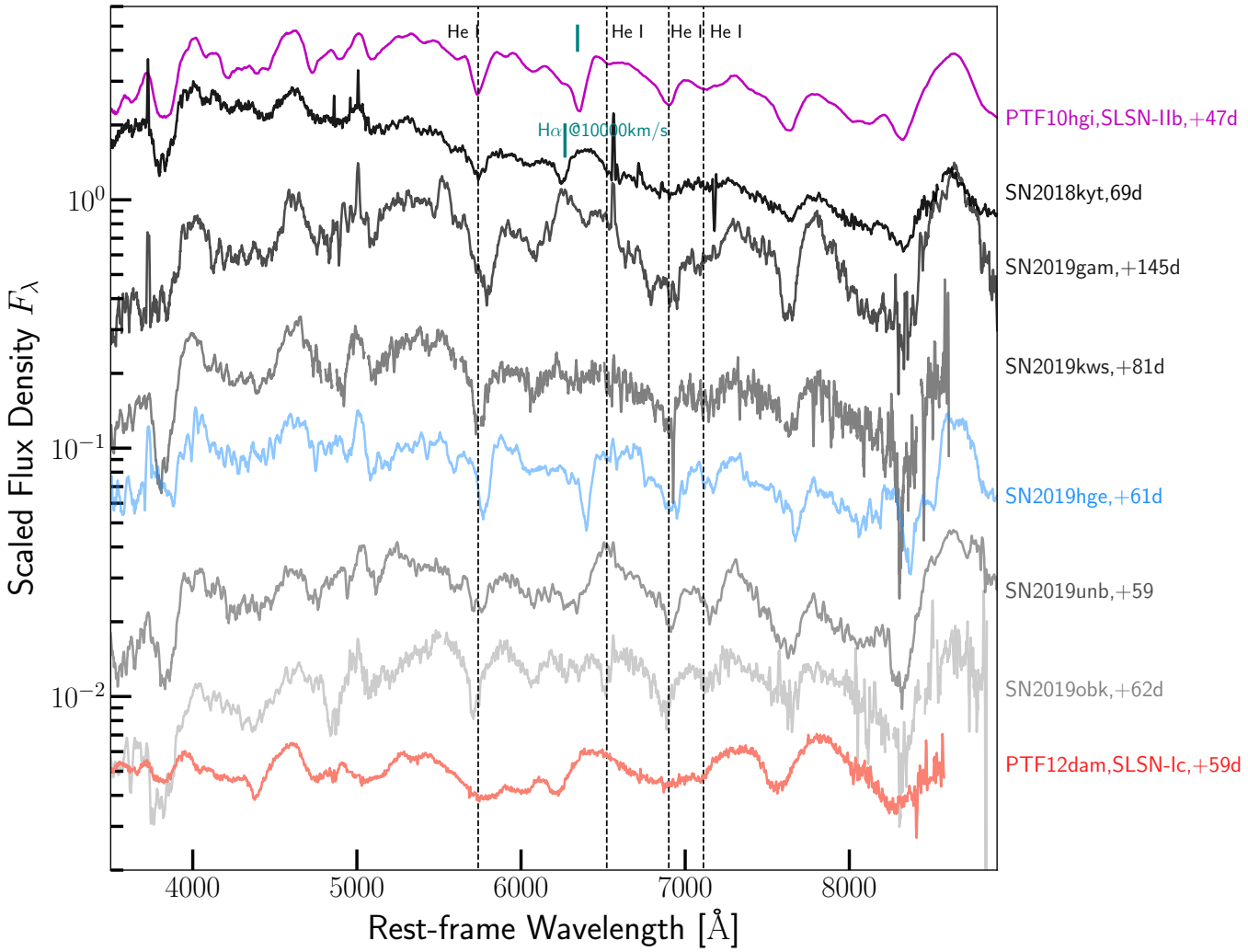

Figure 3. The post-peak spectra for a set of ZTF SLSN-I are displayed in comparison with that of SN2019hge, PTF10hgi, a SLSN-IIb and PTF12dam, a SLSN-I.

netar energy is transported and thermalized to the outer layers are not understood. The recent 3D magnetar simulation by Chen et al. (2020) has examined the dynamical processes, suggesting that Rayleigh Taylor instability can quickly drive Ni and Fe to the outer layers. However, their work does not include simulated spectra. It is likely that Fe-group elements will make the spectra too red. Finally, ejecta-CSM interaction is also a possible solution. The observed LC undulations may support this scenario. However, the LC undulations may be also related to the ejecta clumpiness and changes in opacity.

An important question is why only a small fraction of SLSN-I have He I features. Is the fraction of progenitors retaining some helium at the time of the explosion intrinsically small? If true, this would suggest very efficient mass loss mechanisms. If massive stars are mostly in binaries, stripping by the secondary accretion is certainly more efficient than wind mass loss. An alternative scenario is that most SLSN-I progenitors have helium, but only a small fraction show He features in their spectra, either due to lack of excitation energy, or other peculiar physical conditions. Future modeling work may address this question.

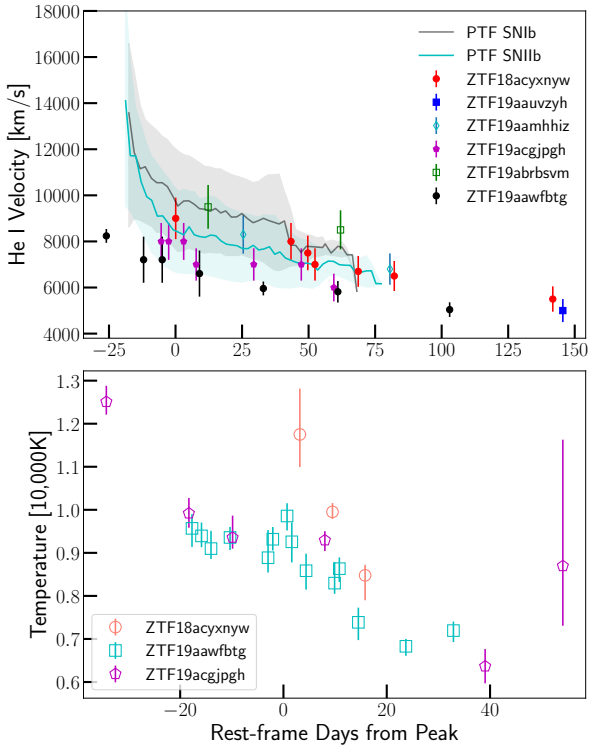

Figure 4. Top: The outflowing velocity of He I λ5876 as a function of time measured for the six SLSN-Ib/IIb. **Bottom:** The modified blackbody temperatures measured from broad band photometry including one or more UV-bands.

Another spectral feature worth noting is that the early phase spectra of these events are blue continuum dominated without obvious O II absorption features. This absence or weak O II can not be explained by the lack of data at early phases because of the spectra at −41 d for SN2019hge (ZTF19aawfbtg) and −28 d for PTF10hgi, nor by low temperatures because the early phase temperatures are high (Figure 4). Spectral smearing due to high velocity is unlikely the main reason because the spectra at the post-peak all show narrow features with relatively low velocities (Figure 1 & 3). Like He I features, the formation of O II absorption requires not only the excitation energy sources to produce ionized O^+, but also are determined by other factors. More spectral modeling is required to understand these factors which make the formation (or absence) of He I and O II absorption features.

Based on observations obtained with the Samuel Oschin Telescope 48-inch and the 60-inch Telescope at the Palomar Observatory as part of the Zwicky Transient Facility project. ZTF is supported by the National Science Foundation under Grant No. AST-1440341 and a collaboration including Caltech, IPAC, the Weizmann Institute for Science, the Oskar Klein Center at Stockholm University, the University of Maryland, the University of Washington, Deutsches Elektronen-Synchrotron and Humboldt University, Los Alamos National Laboratories, the TANGO Consortium of Taiwan, the University of Wisconsin at Milwaukee, and Lawrence Berkeley National Laboratories. Operations are conducted by COO, IPAC, and UW. The Liverpool Telescope is operated on the island of La Palma by Liverpool John Moores University in the Spanish Observatorio del Roque de los Muchachos of the Instituto de Astrofisica de Canarias with financial support from the UK Science and Technology Facilities Council. SED Machine is based upon work supported by the National Science Foundation under Grant No. 1106171. The ZTF forced-photometry service was funded under the Heising-Simons Foundation grant #12540303 (PI: Graham). This work uses the GROWTH Followup Marshal (Kasliwal et al. 2019) and was supported by the GROWTH project funded by the National Science Foundation under Grant No 1545949. A.A.M. is funded by the Large Synoptic Survey Telescope Corporation, the Brinson Foundation, and the Moore Foundation in support of the LSSTC Data Science Fellowship Program; he also receives support as a CIERA Fellow by the CIERA Postdoctoral Fellowship Program (Center for Interdisciplinary Exploration and Research in Astrophysics, Northwestern University). R.L. is sup-

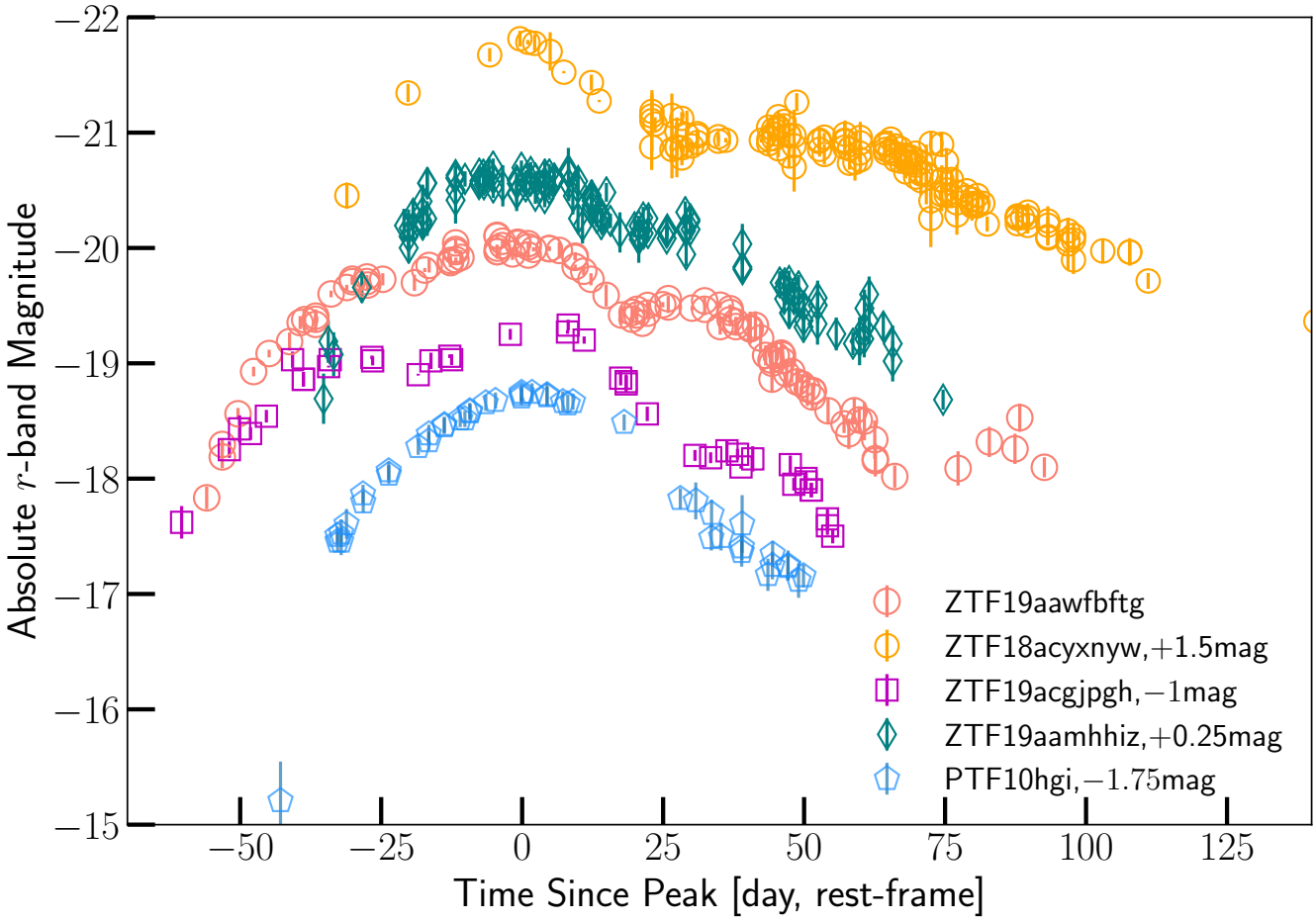

Figure 5. The r-band LCs of the five SLSN-Ib with good phase coverage.

ported by a Marie Skłodowska-Curie Individual Fellowship within the Horizon 2020 European Union (EU) Framework Programme for Research and Innovation (H2020-MSCA-IF-2017-794467).

References

Bellm, E. C., & Sesar, B. 2016, pyraf-dbsp: Reduction pipeline for the Palomar Double Beam Spectrograph
Bellm, E. C., Kulkarni, S. R., Graham, M. J., et al. 2019, PASP, 131, 018002
Blagorodnova, N., Neill, J. D., Walters, R., et al. 2018, PASP, 130, 035003
Chen, K.-J., Woosley, S. E., & Whalen, D. J. 2020, ApJ, 893, 99
Chen, T. W., Nicholl, M., Smartt, S. J., et al. 2017, A&A, 602, A9
Cushing, M. C., Vacca, W. D., & Rayner, J. T. 2004, PASP, 116, 362
De Cia, A., Gal-Yam, A., Rubin, A., et al. 2018, ApJ, 860, 100
Dessart, L. 2019, A&A, 621, A141
Dessart, L., Hillier, D. J., Waldman, R., et al. 2012, MNRAS, 426, L76
Filippenko, A. 1997, ARA&A, 35, 309
Folatelli, G., Contreras, C., Phillips, M. M., et al. 2006, ApJ, 641, 1039
Gal-Yam, A. 2012, Science, 337, 927
Graham, M. J., Kulkarni, S. R., Bellm, E. C., et al. 2019, PASP, 131, 078001
Howell, D. A., Kasen, D., Lidman, C., et al. 2013, ApJ, 779, 98
Hunter, D. J., Valenti, S., Kotak, R., et al. 2009, A&A, 508, 371
Inserra, C., Smartt, S., Jerkstrand, A., et al. 2013, ApJ, 770, 128

Kasen, D., & Bildsten, L. 2010, ApJ, 717, 245
Kasliwal, M. M., Cannella, C., Bagdasaryan, A., et al. 2019, PASP, 131, 038003
Law, N. M., Kulkarni, S. R., Dekany, R. G., et al. 2009, PASP, 121, 1395
Lucy, L. B. 1991, ApJ, 383, 308
Masci, F. J., Laher, R. R., Rusholme, B., et al. 2019, PASP, 131, 018003
Mazzali, P. A., Sullivan, M., Pian, E., et al. 2016, MNRAS, 458, 3455
Modjaz, M., Blondin, S., Kirshner, R. P., et al. 2014, AJ, 147, 99
Nicholl, M., Berger, E., Margutti, R., et al. 2017, ApJL, 845, L8
Oke, J. B., & Gunn, J. E. 1983, ApJ, 266, 713
Oke, J. B., Cohen, J. G., Carr, M., et al. 1995, PASP, 107, 375
Perley, D. A. 2019, PASP, 131, 084503
Planck Collaboration, Aghanim, N., Akrami, Y., et al. 2018, arXiv, arXiv:1807.06209
Quimby, R. M., Aldering, G., Wheeler, J. C., et al. 2007, ApJL, 668, L99
Quimby, R. M., Kulkarni, S. R., Kasliwal, M. M., et al. 2011, Nature, 474, 487
Quimby, R. M., De Cia, A., Gal-Yam, A., et al. 2018, ApJ, 855, 2
Rigault, M., Neill, J. D., Blagorodnova, N., et al. 2019, A&A, 627, A115
Taubenberger, S., Navasardyan, H., Maurer, J. I., et al. 2011, MNRAS, 413, 2140
Vacca, W. D., Cushing, M. C., & Rayner, J. T. 2003, PASP, 115, 389
Wilson, J. C., Henderson, C. P., Herter, T. L., et al. 2004, Society of Photo-Optical Instrumentation Engineers (SPIE) Conference Series, Vol. 5492, Mass producing an efficient NIR spectrograph, ed. A. F. M. Moorwood & M. Iye, 1295
Woosley, S. E. 2017, ApJ, 836, 244
Woosley, S. E., Blinnikov, S., & Heger, A. 2007, Nature, 450, 390
Yan, L., Perley, D. A., De Cia, A., et al. 2018, ApJ, 858, 91
Yan, L., Quimby, R., Ofek, E., et al. 2015, ApJ, 814, 108
Yan, L., Lunnan, R., Perley, D. A., et al. 2017a, ApJ, 848, 6
Yan, L., Quimby, R., Gal-Yam, A., et al. 2017b, ApJ, 840, 57
Yao, Y., Miller, A. A., Kulkarni, S. R., et al. 2019, ApJ, 886, 152

Table 1. A Sample of ZTF SLSN-Ib/IIb

Name	IAU Name	RA	DEC	z	M_g
PTF10hgi	...	16:37:47.04	+06:12:32.3	0.0985	-20.2[a]
ZTF18acyxnyw	SN2018kyt	12:27:56.23	+56:23:35.6	0.108	-20.18
ZTF19aamhhiz	SN2019kws	14:15:04.46	+50:39:06.8	0.1977	-20.17
ZTF19aauvzyh	SN2019gam	10:19:18.32	+17:12:42.6	0.1235	...[b]
ZTF19aawfbtg	SN2019hge	22:24:21.20	+24:47:17.1	0.0866	-19.85
ZTF19acgjpgh	SN2019unb	09:47:57.02	+00:49:36.0	0.0635	-20.13
ZTF19abrbsvm	SN2019obk	22:33:54.08	-02:09:42.3	0.1656	-19.82

NOTE—**a**: The number is from De Cia et al. (2018). **b**: No data within 100 days around the peak.